Heliyon 5 (2019) e01907

Contents lists available at ScienceDirect

Heliyon

journal homepage: www.heliyon.com

Echographic and physical characterization of albumin-stabilized nanobubbles

Akiko Watanabe, Hong Sheng, Hitomi Endo, Loreto B. Feril, Yutaka Irie, Koichi Ogawa, Seyedeh Moosavi-Nejad, Katsuro Tachibana *

Department of Anatomy, Fukuoka University School of Medicine, Fukuoka, 814-0180, Japan

ARTICLE INFO

Keyword:
Nanotechnology

ABSTRACT

There has been increasing interest in using nanobubbles (NBs) for ultrasound mediated drug delivery as well as for ultrasound imaging. Albumin NBs are especially attractive for its potential of becoming a versatile platform for drug carriers and molecular targeted therapy agents. However, physical characterization of NBs is generally considered to be difficult due to various technical issues, such as concentration limitations, nanoparticle contamination, etc. In the present study, we measured the size distribution, concentration and weight density of albumin stabilized NBs by means of multiple nanoscale measurement modalities. Laser nanoparticle tracking analysis, multicolor flow cytometry, resonance mass evaluation showed consistent measurement results of the NBs with low mass weight density and diameter size ranging from 100 nm to 400 nm. Furthermore, the NB solution showed excellent images by high frequency ultrasound (30–50 MHz) in flow model acoustic phantoms. The NBs also induced acute cell disruption by low intensity ultrasound (0.8 W/cm^2) irradiation. We successfully fabricated and characterized albumin stabilized NBs which could serve as an effective platform for future theranositic agents.

1. Introduction

Application of microbubbles is a promising strategy for ultrasound mediated drug delivery as well as for ultrasound imaging [1, 2, 3, 4, 5]. Recent experiments have demonstrated opening of the blood-brain barrier using focused ultrasound in the presence of lipid-based microbubbles. Bubble collapse or oscillation is said to be essential in inducing this phenomenon [6, 7]. Albumin-based bubbles are also attractive for its multiple beneficial features such as, non-antigenicity, biodegradability, easy preparation, biocompatible, and nontoxicity. Additionally, albumin has a potential of becoming a versatile platform for many types of molecular targeted therapy agents bounded by ionic interaction, or dispersing in the albumin particle matrix [8, 9]. Various biomolecules such as antibodies can be conjugated onto the surface of albumin to offer active targeted diagnosis or treatment of cancers.

We recently reported on the cavitation-threshold and rheological parameters of albumin stabilized bubbles in the nanoscale range [10]. It was suggested that these nanobubbles (NBs) could be used as efficient cavitation nuclei with low intensity ultrasound. In theory, nanoscale gas-filled bubbles, sometimes referred as ultra-fine bubbles, have greater potential for being used as a contrast enhanced ultrasound imaging agent as well as for enhancing drug penetration into various tissue with cavitation [11, 12, 13, 14, 15, 16, 17, 18, 19, 20, 21]. Nanoscale bubbles may provide increased intracellular drug delivery by the so-called enhanced permeability and retention (EPR) effect [22, 23, 24, 25], and possible release and/or accumulate of bubbles in the local targeted region, thus enhancing action by addition of ultrasound energy to kill or disrupt cancer cells near the NBs [26, 27, 28, 29, 30, 31]. In spite of these high expectations, research has often been hampered due to the fact that nanobubbles are notoriously difficult to observe and analyze [32]. Differentiating between nanoparticles and nanobubbles is a crucial factor when discussing its application for ultrasound imaging and drug delivery. In order to overcome this key scientific question, a new system was introduced in the present study to accurately measure and characterize albumin stabilized NBs from various aspects. We evaluated the physical properties of these NBs in great detail by combining the following multiple nanoscale measurement modalities; laser nanoparticle tracking analysis, multicolor flow cytometry, resonance mass measurement and high frequency ultrasound imaging. In addition, for the purpose of evaluating the effect of NBs to living cells, *in vitro* cell disruption experiments were conducted by therapeutic ultrasound in the presence of our fabricated albumin stabilized NBs.

* Corresponding author.
E-mail address: k-tachi@fukuoka-u.ac.jp (K. Tachibana).

https://doi.org/10.1016/j.heliyon.2019.e01907
Received 25 December 2018; Received in revised form 26 March 2019; Accepted 3 June 2019

2. Materials and methods

2.1. Preparation of nanobubbles

The human serum albumin NBs were fabricated by high speed agitation method. The agitation device was originally designed as a shaker type tissue homogenizer that provides a 3 dimensional multi-directional motion to a fluid container (Precellys Evolution; Bertin Instruments, France). Two materials (liquid and gas) were placed within a custom made container and agitated at high speeds with this homogenizer device. Briefly, a 700 μl sterile solution of 0.25% human serum albumin (fraction V, purity 96%; Aventis Behring L.L.C., IL, USA) in phosphate-buffered saline (PBS; 140 mM NaCl, 2.7 mM KCl, 10 mM Na2HPO4 and 1.8 mM KH2 PO4, pH 7.4; Cosmo Bio Co., Tokyo, Japan) was added in an air filled 2 ml plastic tube shaped container (height; 30 mm, external diameter; 10 mm). After air tight sealing, the air within the container was replaced with 1 mL of perfluoropropane (C3F8; Takachiho Chemical Industrial Co., Tokyo, Japan) gas using a 23-gauge needle inserted through a small 1 mm hole on the customized 3D printer manufactured cap sealing the container. A silicon sheet (1mm thick) was placed between the cap and the container to prevent air leak. All procedures were carried out within a clean bench to avoid nanoparticle contamination. The container filled with albumin included PBS solution and C3F8 gas was then placed within the previously described homogenizer device. A total of 6 phases of high-speed shaking were performed under the following conditions; 6500 rpm, 10 sec duration, 20 sec pause between each shaking phase. To extract uniform sized NBs from the agitated solution, the containers were centrifuged (MX-301; TOMY, Tokyo, Japan) at 100 g for 5 minutes to separate all microbubbles and the NBs. The NBs included solution was then preserved in a 4 °C condition until measument. Fig. 1 shows the schema of the albumin nanobubble fabrication procedure.

2.2. Nanoparticle tracking analysis

The particle size of albumin NBs was measured by nanoparticle tracking analysis (NTA) device (NanoSight LM10; Malvern Instruments Ltd, Worcestershire, UK). The nanoparticle suspension was illuminated by a 638nm wave length red laser. The nanoparticle movement was visualized by light scattering and the Brownian motion recorded by a CCD camera (C11440-50B; Hamamatsu Photonics K.K., Shizuoka, Japan). This system automatically detects the center position of nanoparticles and tracks each particle motion in a two-dimensional plane for later calculation of the average moving distance under Brownian motion. The image of particle movement under Brownian motion was recorded for 60 sec at room temperature. The range of particle size measurement of NTA method was adjusted from 10 nm to 1000 nm. The particle size was estimated by the average moving distance to the Stokes-Einstein equation. The NBs suspension of 0.5 mL was injected to the sample measurement chamber of the Nanosight system with a 1.0 mL volume plastic syringe (Terumo Co., Tokyo, Japan). Sample image capturing and data analysis were performed using the application software (NTA 3.2 Dev Build 3.2.16). All experiments were performed independently for each sample. Particle size was presented as a mean and mode ± standard error of the average of 3 measurements.

2.3. Flow cytometric analysis

The size and number of albumin NBs were measured by a flow cytometer (CytoFLEX; Beckman Coulter, CA, USA). The flow cytometer was equipped with a 405 nm (violet) laser to detect the particles. The flow cytometer was set up to measure the Side Scatter (SS) from the violet laser for enhanced nanoparticle detection. The Violet-SS signal resolution for particle detection was less than 200 nm. Superior resolution can be obtained with SS than the Forward Scatter (FS) signal and is suitable for measurement of small particles (e.g. nanoscale particles). In order to relate Violet-SS to a particle size, we calibrated the flow cytometer with beads of known size [33, 34]. The polystyrene standard beads (200, 350, and 800 nm; qNano Calibration Particles; Izon Science Ltd, Christchurch, New Zealand, 500 and 1000 nm; Archimedes Standard polystyrene beads; Malvern Instruments Ltd, Worcestershire, UK) was suspended in ultrapure water and measured beforehand with the flow cytometer. The acquired Violet-SS signals of albumin NBs were then analyzed by CytExpert analysis software version 2.0 (Beckman Coulter, CA, USA). A gate was created based on the size of standard beads in the range from 200 nm to 1000 nm for determining the size of our fabricated albumin NBs.

2.4. Resonance mass measurement

The particle mass of albumin NBs were measured by Resonance Mass Measurement (RMM) System (Archimedes; Malvern Instruments Ltd, Worcestershire, UK). The RMM is employed such that the sample solution is passed through a microfluidic flow channel inside a cantilever. Particles that pass through the microfluidic flow channel were detected due to a momentary shift in the resonant frequency of the cantilever associated with the change in mass caused by the passage of a particle of differing density than the solution. The direction of the frequency shift clearly distinguishes particles that have positive buoyancy or negative buoyancy [35, 36]. The resonator in the Archimedes Hi-Q nano sensor (Malvern Instruments Ltd, Worcestershire, UK) with internal microfluidic flow channel dimensions of $2 \times 2\ \mu m^2$ was used in our experiments. For all measurements, the limit of detection, or a threshold of 0.01 Hz was manually selected based on observed baseline noise in control samples of PBS solution. The NBs suspension was supplied to the Hi-Q nanosensor and the measurement was continued for 20 min at room temperature. The buoyant mass was calculated from the transitory resonant frequency shift by using Particle Lab Software version 1.9.81 (Malvern Instruments Ltd, Worcestershire, UK).

2.5. In vitro ultrasound image characterization

Flow phantoms (Fig. 2A and B) consisting of a square shape container ($20 \times 30 \times 20\ mm^3$) of acrylic resin filled with ultrasound gel pad (Aquaflex ultrasound gel pad; Parker lab, NJ, USA) were custom made for the ultrasound contrast-enhanced imaging experiment setup. An acoustically transparent cylindrical shape tube (inner diameter: 2.5 mm, thickness: 0.038 mm, Palladium™ Pebax® Heat shrink tubing; Cobalt

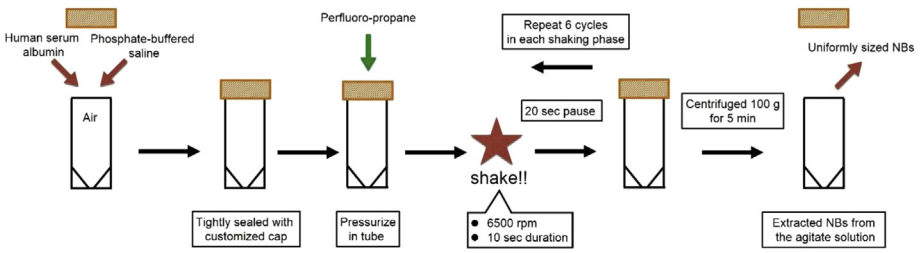

Fig. 1. Schema of the albumin NB fabrication process.

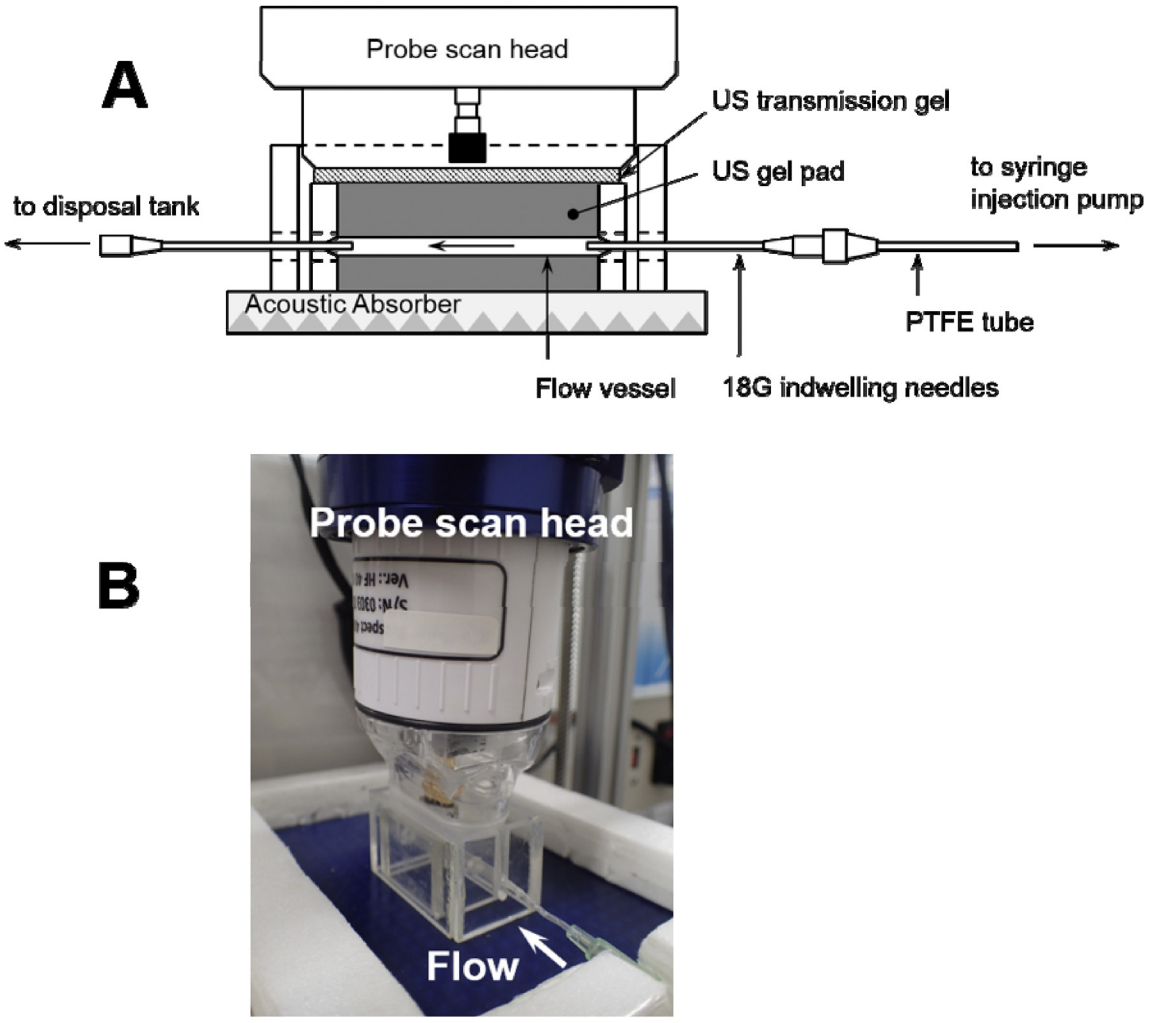

Fig. 2. The flow model phantom. (A) Flow phantom and measurement set up. (B) Snapshot of the flow model phantom and ultrasound probe.

Polymers, CA, USA) were used as a blood vessel-mimicking tube. This flow vessel was placed into ultrasound gel pad container. Two outer cylinder needles of 18-gauge indwelling needles (tube connector) were inserted into the lumen at either end of flow vessel and fixed at either end of tube. By connecting the PTFE tube (outer diameter: 1.6 mm, inner diameter: 0.5 mm, ISIS Co, Osaka, Japan) to the tube connector, the albumin NBs suspension described previously (0.25% human serum albumin) was supplied into a flow vessel at a constant speed rate of 0.3 ml/min by a syringe injection pump (YSP-201; YMC Ltd, Kyoto, Japan). Acoustic evaluation of NBs were performed by a high resolution ultrasound imaging system (Prospect; S-sharp Co, New Taipei city, Taiwan) with a single element mechanical scan probe (PB-406: S-sharp Co, New Taipei city, Taiwan) which had a center frequency of 40 MHz for capturing the images of the albumin NB contrast agent. The ultrasound probe was placed and fixed on the top surface of flow phantom with ultrasound transmission gel (AQUASONIC® 100, Parker labs, NJ, USA) between the probe and phantom. An acoustic absorber was placed beneath the phantom (HAM A; National Physical Laboratory, Middlesex, UK) to eliminate reflection and acoustic artifacts. Ultrasound B-mode images of the ultrasound flow phantom were acquired with the ultrasound probe operated at the frequencies ranging from 30 MHz to 50 MHz, transmission power of 35.5%, frame rate of 5 fps, cycle of 3, dynamic range of 60 dB and gain of 14 dB. Enhanced signal intensities as a function of time in the lumen of the flow vessel was obtained in the B mode images.

2.6. Cell culture

Oral squamous carcinoma cell line HSC-2 was purchased from JCRB (Japanese Collection of Research Bioresources) cell bank and cultured in Minimum Essential Medium (MEM; Nacalai Tesque, Kyoto, Osaka, Japan) with 10% Fetal Bovine Serum (Invitrogen Co., Tokyo, Japan). Cells were maintained at 37.0 °C in humidified air with 5% CO_2. HSC-2 cells collected by trypsin–EDTA (Gibco, NY, USA) were washed and maintained in fresh medium immediately before each sonication experiment. On the day of experiment, cells were collected and centrifuged at 100 g for 5 min. Cell line were free of viral pathogens with initial viability of more than 99% before use in the actual experiments.

2.7. Cell viability measurement

The number of viable HSC-2 cells was measured immediately after all treatments using a trypan blue dye exclusion method. The cell suspensions were mixed with an equal volume of trypan blue stain (0.4%). We considered that both dead and dying cells stained with trypan blue are nonviable, and that the cells not stained with trypan blue as viable. The number of viable cells was counted with a fully automated cell counter (Automated cell counter TC20; BioRad, CA, USA) that uses multi-focal plane imaging analysis for live/dead cells. The survival rate of treated cells was calculated as the ratio of the number of treated surviving cells to the number of non-treated surviving cells. Each treated cell survival rate

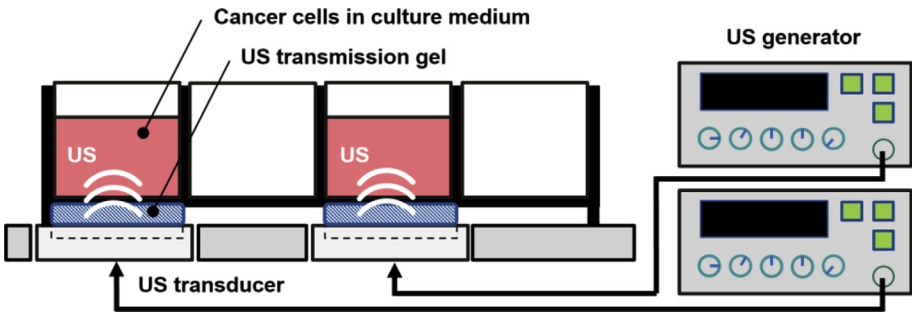

Fig. 3. Schema of the ultrasound cell irradiation experimental set up.

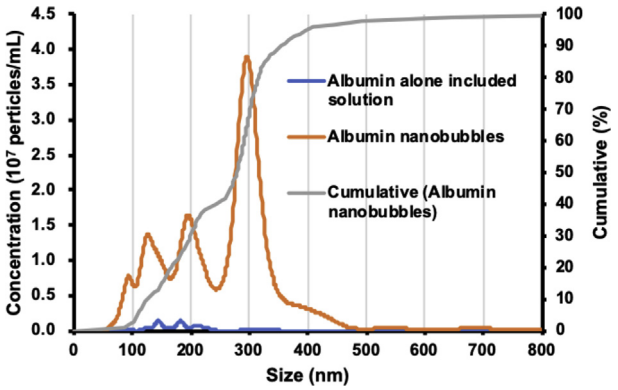

Fig. 4. Characterization of albumin nanobubbles by nanoparticle tracking analysis method. Size distribution of NB diameter (nm). Control sample of the solution of human serum albumin in PBS (blue), albumin NBs (orange), and cumulative curve of albumin NBs (gray).

data consisted of four repeated samples (n = 4).

2.8. Therapeutic ultrasound apparatus and irradiation protocol

Cancer cell line HSC-2 was sonicated in culture multi-wells. The ultrasound condition and NBs concentration were based on experiments previously described [5, 37]. The ultrasound exposure system (Fig. 3) consists of 4 independent ultrasound generators (KTAC-4000; NepaGene, Chiba, Japan) and 4 unfocused 20mm-diameter ultrasound transducers (KP-S20; NepaGene, Chiba, Japan). The 24-well cell culture plate (Lumox® multiwell 24; SARSTEDT, Nümbrecht, Germany) was placed on the acoustic radiation surface of ultrasound transducers via ultrasound transmission gel (Aquasonic 100; Parker lab, NJ, USA). The plate bottom consists of a 50μm thick polystyrene acoustically transparent film described elsewhere [38] for sufficient ultrasound exposure. The ultrasound transducers were driven by different generators at the driving frequency of 1.0 MHz, burst rate of 10 Hz and duty ratio of 50%, and the ultrasound were generated simultaneously from the transducers. Ultrasound energy with 3 acoustic intensities I_{spta} (spatial peak temporal average) of 0.8, 0.9 and 1.0 W/cm^2 (150 kPa, 160 kPa, 170 kPa, respectively) were exposed simultaneously to the 4 wells of the 24 well cell culture plate for 15 second. The 4 wells were sonicated in the same acoustic conditions by placing each of the multiple plates so that the wells of interest were perfectly centered above the 4 transducers. Thermal change near the transducer were monitored by a digital meter connected to one of the four transducers which showed reading below 25 °C at all times.

HSC-2 cells were re-suspended in fresh MEM medium with 10% FBS at a final concentration of 1×10^6 cells/mL. 1.5 mL of cell suspension was added to the each well of the 24-well cell culture plate. 500 μL of NBs included solution was added to the cell suspension in each well. The total volume of both liquids (cell suspension and NBs) was 2 mL in each well. After 5 minutes incubation, ultrasound was exposed to the mixture of HSC-2 cells and NBs. Ultrasound irradiation experiment consisted of three groups: non-treated control, ultrasound alone, albumin NBs combined with ultrasound. After ultrasound irradiation treatment, HSC-2 cells were collected immediately from each well of the 24-well cell culture plates. Trypan-blue dye exclusion test was performed immediately for measurement of cell survival rate.

2.9. Statistics

Measurement data were displayed as mean ± standard deviation (SD). Data was analyzed using unpaired t-test including Welch's correction. The statistical significant differences between various groups were analyzed using SPSS software (IBM, NY, USA). The probability value of $p < 0.05$ was considered statistically significant.

3. Results

3.1. Nanobubble characterization

The size distribution data of the albumin NBs obtained from NTA is shown in Fig. 4. The mean size of control sample of the human serum albumin suspended in PBS solution was 187.6 ± 11.0 nm. The average albumin NB size was 259.4 ± 9.7 nm Fig. 5 shows the flow cytometry albumin NB measurement results. Violet-SS signal intensity histogram of the control sample of albumin alone solution and the albumin stabilized NBs are shown in Fig. 5A and B. The overlaid Violet-SS signal intensity histogram of albumin alone solution and albumin NB are shown in Fig. 5C. The number of albumin NBs and the control albumin having the same scattered Violet-SS signal intensity were correlated against standard known particles size ranging from 200 to 1000 nm. The albumin NBs showed a unimodal distribution and the number of albumin NBs at a relative size of 350 nm (modal diameter) was 2.4-fold greater than that at the relative size of 200 nm. The total number of albumin NBs in size from 200 to 1000 nm was approximately 2.5×10^5 particles, which was approximately 20-fold compared with albumin included solution.

Fig. 6 plots the buoyant mass distributions of albumin NBs obtained by the RMM system. Both the human serum albumin (particle density of 1.03 g/cc) and the albumin NBs (assuming particle density of 0.001 g/cc for air) have positive and negative buoyant masses in PBS (fluid density of 1.0 g/cc). Both mean buoyant mass and particle count of albumin NBs (5775 particles weighed with an average positive buoyant mass of -0.669 fg and 5862 particles weighed with an average negative buoyant mass of 0.671 fg) increased compared to the albumin alone included solutions (3487 particles weighed with an average positive buoyant mass of -0.635 fg and 2986 particles weighed with an average negative buoyant mass of 0.649 fg).

3.2. In vitro ultrasound imaging

Ultrasound imaging in a flow phantom was carried out in order to examine the echogenicity of the albumin NBs. Fig. 7A, B and C shows

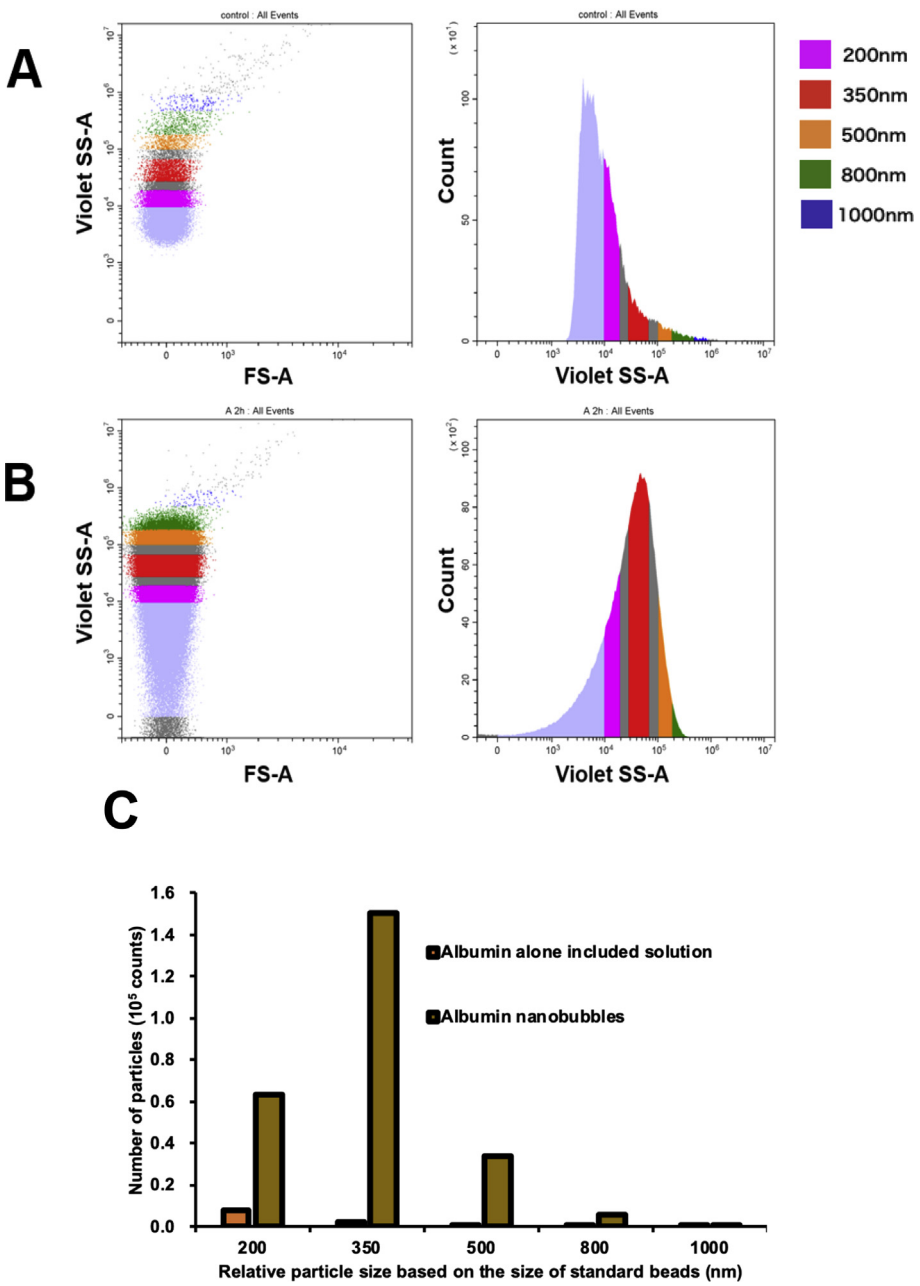

Fig. 5. Characterization of albumin nanobubbles by flow cytometric analysis. Violet- SS signal intensity histogram of human serum albumin alone included solution (A), and the albumin nanobubbles (B). Relative particle size based on the size of standard beads are shown as 200 nm (violet), 350 nm (red), 500 nm (orange), 800 nm (green), and 1000 nm (blue). (C) Comparison of the number of the albumin NBs and control solutions at various size range.

ultrasound images before injection of albumin NBs at driving frequency of 30 MHz, 40 MHz and 50 MHz, respectively. Flow vessel within ultrasound gel pad could be characterized by high frequency ultrasound imaging in the range from 30 to 50 MHz. Immediately after NB injection, NBs were detected as high echo area while enhancement was obtained within the flow vessel lumen by B-mode imaging (Fig. 7D, E and F). The region of interest (ROI) was created within the flow vessel lumen. Time signal intensity curve (TIC) on the lumen of the flow vessel at various ultrasound driving frequencies are shown in Fig. 7G. Note that the gray scale intensity is subtracted from the initial value from after injection of albumin NBs. Gray scale intensity during the wash-in phase increased from baseline to peak intensity (PI) in approximately 400 frames. Immediately after washing with PBS, gray scale intensity during the wash-out phase decreased from PI to baseline. Several ultrasound perfusion parameters were derived from TIC: PI and the area under the curve (AUC) from parameters of relative blood volume and mean transit time (MTT). The time to peak intensity (TTP) was obtained from the parameter of blood flow velocity [39, 40]. Comparison of perfusion parameters for albumin NBs at various NBs concentrations were derived from TIC in the lumen of flow vessel summarized in Table 1. It was observed that the PI and AUC value declined as with decreasing the NBs concentration between the range from 1/20 to 1/200.

3.3. Cell disruption by NBs under ultrasound irradiation

The effects of ultrasound alone and enhanced cell disruption by ultrasound in the presence of NBs at various irradiation intensities to HSC-2 cells are shown in Fig. 8. Cell killing rate of HSC-2 cells after ultrasound treatment at 0.8 W/cm^2, 0.9 W/cm^2, 1.0 W/cm^2 were 2.8 ± 4.2%, 14.1 ± 4.6% and 27.1 ± 3.9%, respectively. The cell killing rate tended to

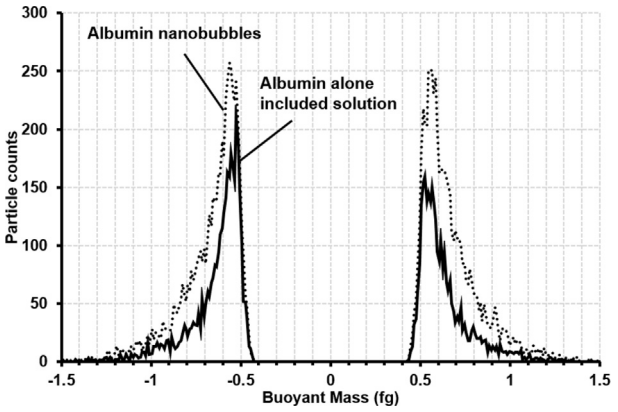

Fig. 6. Buoyant mass distributions of albumin nanobubbles measured by resonance mass measurement system. Control sample of human serum albumin alone included solution (solid line), and albumin stabilized NBs (dotted line).

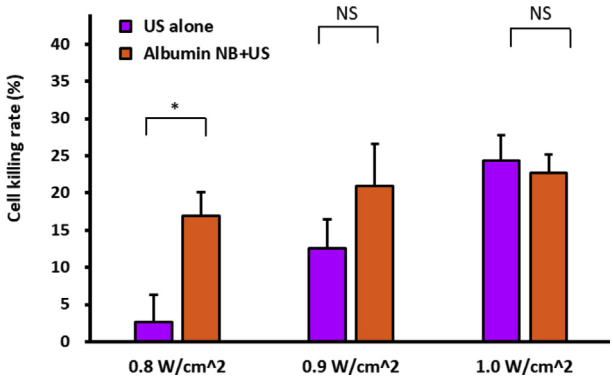

Fig. 8. Comparison of cell killing rate after irradiation at various ultrasound intensities. Each data point represents mean ± SD (N = 4, *p < 0.05, NS: not significant).

increase with increased ultrasound irradiation intensities and shows statistically significant differences compared to each ultrasound intensity ($p < 0.05$). In order to investigate whether ultrasound in the presence of NBs could enhance HSC-2 cells killing, we compared the cell killing effect in the presence/absence of NBs to HSC-2 cells under various ultrasound intensities.

Cell killing rate with ultrasound treatment at intensities 0.8 W/cm^2, 0.9 W/cm^2 and 1.0 W/cm^2 in the presence of NBs were 18.9 ± 3.5%, 23.6 ± 6.3%, 25.6 ± 2.8%, respectively. The NBs in combination with ultrasound at 0.8 W/cm^2 increased 6.8-fold higher than the cell killing rate compared to ultrasound alone treated cells ($p < 0.05$). Albumin NBs significantly enhanced the cell killing effect only at low-intensity ultrasound of 0.8 W/cm^2. The raw/processed data required to reproduce these findings cannot be shared at this time due to technical or time limitations.

4. Discussion

We successfully characterized the physical properties of albumin-stabilized nanobubbles using various nanoscale measurement modalities. To our knowledge, this is the first evidence reported regarding detection and measurement of nanoscale human serum albumin gas-filled bubbles. The Resonance mass measurement (RMM) method that we used in the experiment allowed direct measurement of the absolute mass of the nanoparticles. Burg et al [35, 41] indicated that RMM could detect biomolecular (eg fetal bovine serum, IgG antibody) binding inside the microfluidic flow channel of cantilever by measuring resonance frequency shifts caused with the accumulation of nanoscale proteins. For example, they showed that the mass of suspended gold nanoparticles and of living bacteria were heavier than the buffer solution. A single yeast cell was directly measured and characterized during growth by reading

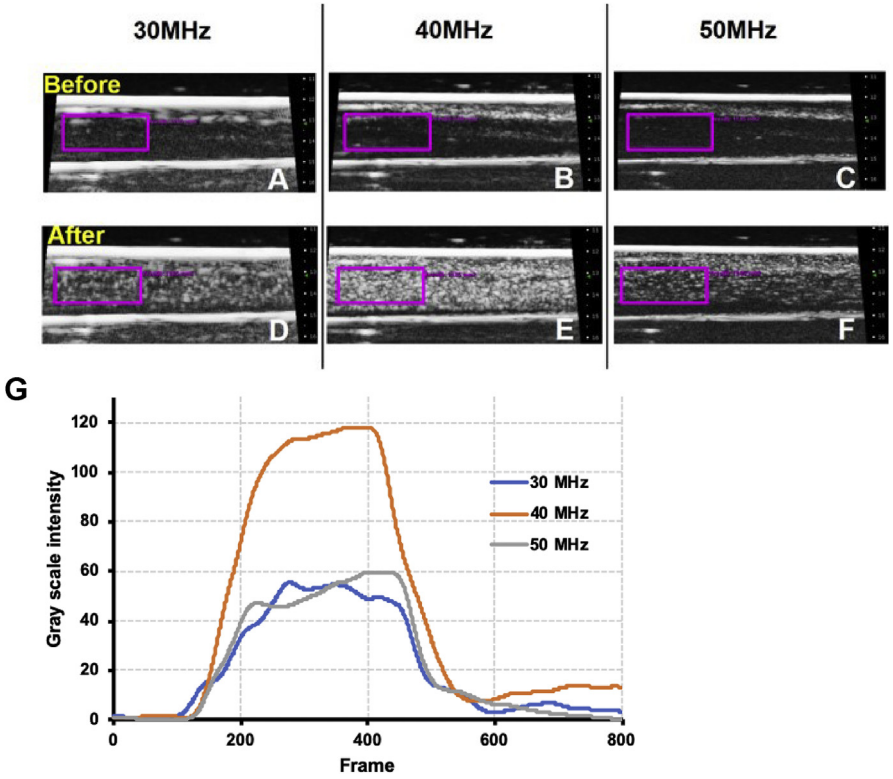

Fig. 7. Ultrasound images from the flow model phantom study. Ultrasound images before and after injection of albumin NBs into the flow vessel. Purple frames shows region of interest area (ROI). (A,D) driving frequency of 30 MHz. (B,E) driving frequency of 40 MHz. (C,F) driving frequency of 50 MHz. (G) albumin NB time-signal intensity curve in the lumen of flow vessel at various ultrasound driving frequencies (Supplementary materials).

Table 1
Comparison of perfusion parameters of albumin nanobubbles at various nanobubbles concentrations derived from time signal intensity curve (TIC) in the lumen of flow vessel. Ultrasound B-mode images of the ultrasound flow phantom were acquired with a 40 MHz ultrasound probe operated at the frequency of 40 MHz, transmission power of 35.5%, frame rate of 5 fps, cycle of 3, dynamic range of 60 dB and gain of 14 dB.

Concentration	1/20	1/80	1/200
AUC	38331.9	12509.1	6791.3
MTT	111	125	118
PI	117.9	38.1	21.9
TTP	147	147	154

Abbreviations: AUC, area under the curve; MTT, mean transit time; PI, peak signal intensity; TTP, time to peak signal intensity.

real-time changes in relative cell density via the direction of change in buoyant mass [42]. The resolution of the 8μm tail RMM used for their experiments was less than 3 fg. A range of 0.1%–2% of a yeast cell density change in a high-density resolution was detected throughout the cell cycle. Nejadnik et al [43] reported that RMM can quantitatively measure the adsorption of protein or antibody to the surface of suspended polystyrene beads which leads to increase in the buoyant mass. As to measurements of NBs, this method has been frequently applied for distinguishing whether the detected particles were a gas, or a solid contaminant [44]. Kobayashi have previously reported that NBs were distinguishable from dust particles (eg solid particles) by reading the direction of particle buoyancy. The dust particles had greater density than that of the liquid surrounding the particles. If particles are detected with a low specific gravity which has smaller density than that of the surrounding liquid, it can be considered as a typical "gas bubble". However, it must be taken into consideration that the presence of nanobubbles will attract nanoparticles at the gas/liquid interface due to the Pickering effect [45]. It is unlikely that the two are totally independent of each other.

In our results, the number of albumin NBs solution with positive buoyant particles which had lower density than PBS solution, increased by 1.7-fold compared to albumin alone included solution. Furthermore, our echography evaluations under physiologically relevant flow conditions suggests that the echogenic signals of the albumin NBs were detectable and sufficient for acoustic enhancement within small blood vessel-mimicking flow tube phantom at 40 MHz transmission frequency. Albumin NBs at various concentrations were individually characterized from the perfusion parameters derived from TIC analysis. As acoustics signals are very sensitive to the boundary between liquid and gas, we considered that both RMM and echography detected particles within the albumin solution were actually gas-filled bubbles and not dust particles. Calculations of the random Brownian movement from the nanoparticle tracking revealed individual particle size and concentration of the albumin NBs which were similarly predicted by flow cytometric analysis from the light scattering angle pattern of calibrated known particles sizes. The estimated NBs size detected in the suspension ranged from 100 to 400 nm. Particles of similar size were not detected in the control albumin solutions. The number of particles size less than 200 nm that can extravasate to the tumor tissues by EPR effect while avoiding the biological barriers, such as at the liver and the spleen, accounted for 30% of the total number of NBs. The size distribution of albumin NBs were well consistent with the two different NTA and flow cytometric analysis. As our albumin NBs were visualized with ultrasound imaging device, it could be suggested that NBs of this size and concentration are sufficient for possible application in visualizing specific tumor tissues and other organs. However, it should be noted that temperature and pressure change during the course of the experiments might alter the bubble size distribution and echo visibility.

We previously demonstrated that low intensity ultrasound irradiation in conjunction with cetuximab coated albumin microbubbles (MBs) selectively killed and induced apoptosis in EGFR-expressing oral squamous cell [5]. Whereas these MBs is a pure intravascular tracer that will not extravasate from the systemic circulation to the tumor tissues since they cannot cross the blood vessel wall. From the results of particle size and mass measurement as well as the echography study in present study, we postulate a portion of the NBs that were detected within the albumin solution may avoid the organ-level barriers, thus cross the blood vessel wall and efficiently reach tumor cells. However further *in vivo* studies are yet to be performed to come to conclusions.

The exact mechanisms in our cell experiments by which ultrasound specifically killed cancer cells in the presence of NBs are unknown. In recent reports, Adhikari et al [46] performed molecular dynamics simulations in order to understand the mechanism of membrane poration by NB collapse. One of many examples of their numerical stimulations, while in the presence of NB diameter of 60 nm, when the impulse of shock wave at velocity of 2 km/s passes the model membrane creates a negative pressure region on the membrane surface. At the same time, a positive pressure region appears by bubble collapse at the center of membrane. They indicated that unequal distribution of pressure induced from the large differences of 100 MPa between positive and negative pressure sufficiently form membrane pore with the radius of 15 nm. On the other hand, Arita et al [47] experimentally verified that expansion and collapse of cavitation generated by laser irradiated polystyrene nanoparticle (diameter of 500 nm) which optically trapped at distance of 10μm from cell adherent surface inducing the gene transfection followed by a large displacement on the adherent cells. It is suggested that a similar cell killing or disruption phenomenon occurred in our experiments using albumin NBs. Furthermore, we previously reported that similar sized albumin-stabilized NBs (100–250 nm) were sensitive to irradiated ultrasound and were excited easily to low acoustic pressure at frequency range from 3 to 5 MHz [10]. Inertial cavitation was observed by analyzing the noise emission from the albumin NBs where the level of scattered inertial cavitation noise was greater than that of conventional microbubble ultrasound contrast agent Sonazoid®. The present study is consistent with these results from the fact that high sensitivity of albumin NB cell disruption with low ultrasound intensity (less than 0.8 W/cm^2) was observed in our results. It is suggested that NB size ranging from 100 to 400 nm can induce membrane structural change by cavitation thus leading to increased cell killing or disruption of HSC-2 cells. Nevertheless, we demonstrated that our well characterized albumin NBs induced to an extent a biological effect in the presence of ultrasound.

5. Conclusion

We successfully characterized the size distribution, weight density and the concentration of our newly developed albumin stabilized NBs by 3 different nanoscale measurement modalities. Furthermore, the NBs were easily visualized with a 40MHz ultrasound imaging device. In addition, we demonstrated that low intensity ultrasound irradiation in conjunction with these NBs enhanced acute cancer cell disruption *in vitro*. We believe that albumin stabilized NB agents may become a very promising platform for both ultrasound contrast imaging and therapy.

Declarations

Author contribution statement

Akiko Watanbe: Conceived and designed the experiments; Performed the experiments; Analyzed and interpreted the data; Wrote the paper.

Hong Sheng: Performed the experiments; Analyzed and interpreted the data; Wrote the paper.

Hitomi Endo, Lorento B. Feril: Analyzed and interpreted the data.

Yutaka Irie, Seyedeh Moosavi-Nejad: Performed the experiments.

Koichi Ogawa: Analyzed and interpreted the data; Contributed reagents, materials, analysis tools or data.

Katsuro Tachibana: Analyzed and interpreted the data; Contributed reagents, materials, analysis tools or data; Wrote the paper.

Funding statement

This work was supported by SonoCore Inc, Japan (Grant No 160396).

Competing interest statement

The authors declare the following conflict of interests: Katsuro Tachibana; owns stock in SonoCore Inc.

Additional information

Supplementary content related to this article has been published online at https://doi.org/10.1016/j.heliyon.2019.e01907.

Acknowledgements

We thank Ms Akino Akamine and Ms Miki Matsuo for their contribution in fabricating and measuring the NBs.

References

[1] D. Shi, L. Guo, S. Duan, M. Shang, D. Meng, L. Cheng, J. Li, Influence of tumor cell lines derived from different tissue on sonoporation efficiency under ultrasound microbubble treatment, Ultrason. Sonochem. (2017).
[2] F.T.H. Yu, X. Chen, J. Wang, B. Qin, F.S. Villanueva, Low intensity ultrasound mediated liposomal doxorubicin delivery using polymer microbubbles, Mol. Pharm. (2016).
[3] J.M. Escoffre, A. Novell, S. Serrière, T. Lecomte, A. Bouakaz, Irinotecan delivery by microbubble-assisted ultrasound: in vitro validation and a pilot preclinical study, Mol. Pharm. (2013).
[4] B.H.A. Lammertink, C. Bos, R. Deckers, G. Storm, C.T.W. Moonen, J.M. Escoffre, Sonochemotherapy: from bench to bedside, Front. Pharmacol. (2015).
[5] K. Narihira, A. Watanabe, H. Sheng, H. Endo, L.B. Feril, Y. Irie, K. Ogawa, S. Moosavi-Nejad, S. Kondo, T. Kikuta, K. Tachibana, Enhanced cell killing and apoptosis of oral squamous cell carcinoma cells with ultrasound in combination with cetuximab coated albumin microbubbles, J. Drug Target. (2018).
[6] C. Bing, Y. Hong, C. Hernandez, M. Rich, B. Cheng, I. Munaweera, D. Szczepanski, Y. Xi, M. Bolding, A. Exner, R. Chopra, Characterization of different bubble formulations for blood-brain barrier opening using a focused ultrasound system with acoustic feedback control, Sci. Rep. (2018).
[7] N. Lipsman, Y. Meng, A.J. Bethune, Y. Huang, B. Lam, M. Masellis, N. Herrmann, C. Heyn, I. Aubert, A. Boutet, G.S. Smith, K. Hynynen, S.E. Black, Blood–brain barrier opening in Alzheimer's disease using MR-guided focused ultrasound, Nat. Commun. (2018).
[8] J.L. Chen, A.H. Dhanaliwala, A.J. Dixon, A.L. Klibanov, J.A. Hossack, Synthesis and characterization of transiently stable albumin-coated microbubbles via a flow-focusing microfluidic device, Ultrasound Med. Biol. (2014).
[9] F. Kratz, Albumin as a drug carrier: design of prodrugs, drug conjugates and nanoparticles, J. Control. Release (2008).
[10] M. Lafond, A. Watanabe, S. Yoshizawa, S.I. Umemura, K. Tachibana, Cavitation-threshold determination and rheological-parameters estimation of albumin-stabilized nanobubbles, Sci. Rep. (2018).
[11] T. Yin, P. Wang, R. Zheng, B. Zheng, D. Cheng, X. Zhang, X. Shuai, Nanobubbles for enhanced ultrasound imaging of tumors, Int. J. Nanomed. (2012).
[12] J. Li, Y. Tian, D. Shan, A. Gong, L. Zeng, W. Ren, L. Xiang, E. Gerhard, J. Zhao, J. Yang, A. Wu, Neuropeptide Y Y1receptor-mediated biodegradable photoluminescent nanobubbles as ultrasound contrast agents for targeted breast cancer imaging, Biomaterials (2017).
[13] S.A. Peyman, J.R. McLaughlan, R.H. Abou-Saleh, G. Marston, B.R.G. Johnson, S. Freear, P.L. Coletta, A.F. Markham, S.D. Evans, On-chip preparation of nanoscale contrast agents towards high-resolution ultrasound imaging, Lab Chip (2016).
[14] J. Du, X.Y. Li, H. Hu, L. Xu, S.P. Yang, F.H. Li, Preparation and imaging investigation of dual-targeted C3F8-filled PLGA nanobubbles as a novel ultrasound contrast agent for breast cancer, Sci. Rep. (2018).
[15] M. Wu, H. Zhao, L. Guo, Y. Wang, J. Song, X. Zhao, C. Li, L. Hao, D. Wang, J. Tang, Ultrasound-mediated nanobubble destruction (UMND) facilitates the delivery of A10-3.2 aptamer targeted and siRNA-loaded cationic nanobubbles for therapy of prostate cancer, Drug Deliv. (2018).
[16] R.H. Perera, L. Solorio, H. Wu, M. Gangolli, E. Silverman, C. Hernandez, P.M. Peiris, A.M. Broome, A.A. Exner, Nanobubble ultrasound contrast agents for enhanced delivery of thermal sensitizer to tumors undergoing radiofrequency ablation, Pharm. Res. (2014).
[17] R. Cavalli, A. Bisazza, D. Lembo, Micro- and nanobubbles: a versatile non-viral platform for gene delivery, Int. J. Pharm. (2013).
[18] W. Bin Cai, H.L. Yang, J. Zhang, J.K. Yin, Y.L. Yang, L.J. Yuan, L. Zhang, Y.Y. Duan, The optimized fabrication of nanobubbles as ultrasound contrast agents for tumor imaging, Sci. Rep. (2015).
[19] Y.J. Zhang, D.N. Bai, J.X. Du, L. Jin, J. Ma, J.L. Yang, W. Bin Cai, Y. Feng, C.Y. Xing, L.J. Yuan, Y.Y. Duan, Ultrasound-guided imaging of junctional adhesion molecule-A-targeted microbubbles identifies vulnerable plaque in rabbits, Biomaterials 94 (2016) 20–30.
[20] Y. Go, H. Lee, L. Jeong, S. Sun, E. Hong, E. Jung, C. Ko, J. Noh, S. Park, M. Lee, C. Song, D. Lee, Acid-triggered echogenic nanoparticles for contrast-enhanced ultrasound imaging and therapy of acute liver failure, Biomaterials 186 (2018) 22–30.
[21] S. Shen, Y. Li, Y. Xiao, Z. Zhao, C. Zhang, J. Wang, H. Li, F. Liu, N. He, Y. Yuan, Y. Lu, S. Guo, Y. Wang, W. Liao, Y. Liao, Y. Chen, J. Bin, Folate-conjugated nanobubbles selectively target and kill cancer cells via ultrasound-triggered intracellular explosion, Biomaterials 181 (2018) 293–306.
[22] Y. Matsumura, H. Maeda, A new concept for macromolecular therapeutics in cancer chemotherapy: mechanism of tumoritropic accumulatio of proteins and the antitumor agents Smancs, Cancer Res. 46 (1986) 6387–6392.
[23] H. Maeda, Y. Matsumura, Tumoritropic and lymphotropic principles of macromolecular drugs, Crit. Rev. Ther. Drug Carrier Syst. 6 (1989) 193–210.
[24] K.R. Gajbhiye, J.M. Gajbhiye, EPR effect based nanocarriers targeting for treatment of cancer, Int. J. Drug Deliv. 8 (2017) 117–124.
[25] H.S. Min, S. Son, D.G. You, T.W. Lee, J. Lee, S. Lee, J.Y. Yhee, J. Lee, M.H. Han, J.H. Park, S.H. Kim, K. Choi, K. Park, K. Kim, I.C. Kwon, Chemical gas-generating nanoparticles for tumor-targeted ultrasound imaging and ultrasound-triggered drug delivery, Biomaterials 108 (2016) 57–70.
[26] Y. Gao, C. Hernandez, H.X. Yuan, J. Lilly, P. Kota, H. Zhou, H. Wu, A.A. Exner, Ultrasound molecular imaging of ovarian cancer with CA-125 targeted nanobubble contrast agents, Nanomed. Nanotechnol. Biol. Med. (2017).
[27] F. Xie, Z.P. Li, H.W. Wang, X. Fei, Z.Y. Jiao, W.B. Tang, J. Tang, Y.K. Luo, Evaluation of liver ischemia-reperfusion injury in rabbits using a nanoscale ultrasound contrast agent targeting ICAM-1, PLoS One (2016).
[28] H. Yang, W. Cai, L. Xu, X. Lv, Y. Qiao, P. Li, H. Wu, Y. Yang, L. Zhang, Y. Duan, Nanobubble-Affibody: novel ultrasound contrast agents for targeted molecular ultrasound imaging of tumor, Biomaterials (2015).
[29] H. Yang, L. Deng, T. Li, X. Shen, J. Yan, L. Zuo, C. Wu, Y. Liu, Multifunctional PLGA nanobubbles as theranostic agents: combining doxorubicin and P-gp siRNA co-delivery into human breast cancer cells and ultrasound cellular imaging, J. Biomed. Nanotechnol. (2015).
[30] M. Meng, J. Gao, C. Wu, X. Zhou, X. Zang, X. Lin, H. Liu, C. Wang, H. Su, K. Liu, Y. Wang, X. Xue, J. Wu, Doxorubicin nanobubble for combining ultrasonography and targeted chemotherapy of rabbit with VX2 liver tumor, Tumor Biol. (2016).
[31] L.W. Chang, M.L. Hou, S.H. Hung, L.C. Lin, T.H. Tsai, Pharmacokinetics of quercetin-loaded nanodroplets with ultrasound activation and their use for bioimaging, Int. J. Nanomed. (2015).
[32] M. Alheshibri, J. Qian, M. Jehannin, V.S.J.J. Craig, A history of nanobubbles, Langmuir 32 (2016) 11086–11100.
[33] R.M. Zucker, J.N.R. Ortenzio, W.K. Boyes, Characterization, detection, and counting of metal nanoparticles using flow cytometry, Cytom. Part A. (2016).
[34] L. Wisgrill, C. Lamm, J. Hartmann, F. Preißing, K. Dragosits, A. Bee, L. Hell, J. Thaler, C. Ay, I. Pabinger, A. Berger, A. Spittler, Peripheral blood microvesicles secretion is influenced by storage time, temperature, and anticoagulants, Cytom. Part A. (2016).
[35] T.P. Burg, M. Godin, S.M. Knudsen, W. Shen, G. Carlson, J.S. Foster, K. Babcock, S.R. Manalis, Weighing of biomolecules, single cells and single nanoparticles in fluid, Nature (2007).
[36] A.R. Patel, D. Lau, J. Liu, Quantification and characterization of micrometer and submicrometer subvisible particles in protein therapeutics by use of a suspended microchannel resonator, Anal. Chem. (2012).
[37] Y. Ikeda-Dantsuji, L.B. Feril, K. Tachibana, K. Ogawa, H. Endo, Y. Harada, R. Suzuki, K. Maruyama, Synergistic effect of ultrasound and antibiotics against Chlamydia trachomatis-infected human epithelial cells in vitro, Ultrason. Sonochem. (2011).
[38] H. Bruus, Acoustofluidics 2: perturbation theory and ultrasound resonance modes, Lab Chip (2012).
[39] K.G. King, M. Gulati, H. Malhi, D. Hwang, I.S. Gill, P.M. Cheng, E.G. Grant, V.A. Duddalwar, Quantitative assessment of solid renal masses by contrast-enhanced ultrasound with time–intensity curves: how we do it, Abdom. Imag. (2015).
[40] C.F. Dietrich, M.A. Averkiou, J.M. Correas, N. Lassau, E. Leen, F. Piscaglia, An EFSUMB introduction into dynamic contrast-enhanced ultrasound (DCE-US) for quantification of tumour perfusion, Ultraschall Der Medizin (2012).
[41] T.P. Burg, A.R. Mirza, N. Milovic, C.H. Tsau, G.A. Popescu, J.S. Foster, S.R. Manalis, Vacuum-packaged suspended microchannel resonant mass sensor for biomolecular detection, J. Microelectromechanical Syst. (2006).
[42] A.K. Bryan, A. Goranov, A. Amon, S.R. Manalis, Measurement of mass, density, and volume during the cell cycle of yeast, Proc. Natl. Acad. Sci. (2010).
[43] M.R. Nejadnik, W. Jiskoot, Measurement of the average mass of proteins adsorbed to a nanoparticle by using a suspended microchannel resonator, J. Pharm. Sci. (2015).
[44] H. Kobayashi, S. Maeda, M. Kashiwa, T. Fujita, Measurement and identification of ultrafine bubbles by resonant mass measurement method, in: Proceedings Volume 9232, International Conference on Optical Particle Characterization (OPC 2014), 2014, p. 92320S.
[45] Z. Du, M.P. Bilbao-Montoya, B.P. Binks, E. Dickinson, R. Ettelaie, B.S. Murray, Outstanding stability of particle-stabilized bubbles, Langmuir 19 (2003) 3106–3108.
[46] U. Adhikari, A. Goliaei, M.L. Berkowitz, Mechanism of membrane poration by shock wave induced nanobubble collapse: a molecular dynamics study, J. Phys. Chem. B (2015).
[47] Y. Arita, M.L. Torres-Mapa, W.M. Lee, T. Čižmár, P. Campbell, F.J. Gunn-Moore, K. Dholakia, Spatially optimized gene transfection by laser-induced breakdown of optically trapped nanoparticles, Appl. Phys. Lett. (2011).